

Analysis of Conservative and Magnetically Induced Electric Fields in a Low-Frequency Birdcage Coil*

Bu S. Park^{1#}, Sunder S. Rajan¹, Christopher M. Collins², Leonardo M. Angelone¹

¹Division of Physics, Center for Devices and Radiological Health, Office of Medical Products and Tobacco, Food and Drug Administration, Silver Spring, USA; ²Department of Radiology, New York University, New York, USA.
Email: [#]bu.park@fda.hhs.gov

Received May 16th, 2013; revised June 17th, 2013; accepted June 25th, 2013

Copyright © 2013 Bu S. Park *et al.* This is an open access article distributed under the Creative Commons Attribution License, which permits unrestricted use, distribution, and reproduction in any medium, provided the original work is properly cited.

ABSTRACT

Numerical methods are used to evaluate variations of the electromagnetic fields generated by a head-sized birdcage coil as a function of load (“loading effect”). The loading effect was analyzed for the cases of a coil loaded with a conductive cylindrical sample, a dielectric cylindrical sample, and an anatomically precise head model. Maxwell equations were solved by means of finite difference time domain (FDTD) method conducted at 12.8, 64, and 128 MHz. Simulation results indicate that at 12.8 MHz the conservative electric field (E_c) caused by the scalar electric potentials between the coil and the load or within the load was significantly higher than the magnetically-induced electric field (E_i) and was the major component of the total electric field (E_{total}). The amplitudes of E_c and E_{total} are seen to be lower within a sample than at a corresponding location in an empty coil, but approximately 65% higher in the space between coil and sample than at a corresponding location in an empty coil. This is due to polarization effects generating an additional scalar potential parallel to the original field. The increased electric field between coil and sample may cause increased power deposition at the surface of the sample and may affect the RF-induced currents in external leads used for physiological recording, *i.e.* ECG, during MRI scanning.

Keywords: MRI; FDTD; Loading Effect; Conservative Electric Field; Birdcage Coil

1. Introduction

In magnetic resonance imaging (MRI), the signal to noise ratio (SNR) and the specific energy absorption rate (SAR), the dosimetric parameter used to establish safety limits for human subjects by the International Electrotechnical Commission (IEC) [1] and the US Food and Drug Administration [2], depend upon the total electric field (E_{total}). The E_{total} can be decomposed into a conservative and magnetically-induced electric fields (E -fields) [3] and a distinction is often needed between the two components. Conservative E -fields (E_c) caused by the scalar electrical potential on conductors give rise to a portion of sample loss also referred to as “dielectric loss” [4]. Magnetically-induced E -fields (E_i) are created by the time-varying magnetic fields [5], and give rise to a

portion of sample loss also referred to as “inductive loss” [4]. In some cases it is possible to reduce the losses due to E_c without changing the current distribution or magnetic field distribution using a so called “ E_c -shield” [6], and thus maintaining the desired sensitivity and field of view (FOV) while reducing SAR in the sample and/or the noise received from the sample [6-9]. A previous study [6] showed that this method could be applied to a solenoid coil. This study evaluated whether the method of “ E_c -shield” could be also extended to a birdcage coil, the most common type of coil used in human MRI. One of the motivations of this study to understand the mechanism of thermal injury to skin is currently the most common type of adverse event reported for MRI scans [10]. Another reason for this study is to find the effect of a conductive or a dielectric sample related to the safety assurance in a region of interest (ROI), particularly between the RF coil and the sample. Previous research [9,11] showed that the total electric field inside a coil would be decreased with addition of a loading sample.

*Disclaimer: The mention of commercial products, their sources, or their use in connection with material reported herein is not to be construed as either an actual or implied endorsement of such products by the Department of Health and Human Services.

[#]Corresponding author.

Conversely, the hypothesis driving the proposed study was that the electric field decreases only within the loading sample, but it is the same or higher in the space between coil and sample. Changes in electric field between coil and sample may cause increased power deposition in the subject skin, with possible related thermal injury [10]. Moreover, changes in electric field may also affect the RF-induced currents in external leads used for physiological recording during MRI (e.g., ECG or EEG leads). Additionally, there have been some suggestions that E_c may play a significant role in the total sample loss, although it is generally believed that almost all of the sample loss is magnetically-induced [12].

The study was conducted by means of numerical simulations conducting a systematic analysis of the electromagnetic field, including E_c and E_i generated by the birdcage coil within and surrounding the load. The study took advantage of a recently developed method based on quasi-static approximation that allows separating numerically-calculated E -field distributions into conservative and magnetically-induced portions [3]. We performed numerical electromagnetic field simulations within and surrounding a high pass (HP) birdcage coil combined with a cylindrical conductive phantom and a human head model at different frequencies. Additionally, the volume charge density (ρ_v) distribution generating the scalar electric potential and E_c was calculated to support the explanation of electromagnetic field variations. Results were analyzed to evaluate the contribution of E_c , E_i and RF magnetic field (B_1) to the total electromagnetic field distribution.

Conservative and Magnetically-Induced Electric Field

The power loss (P) can be calculated as [8]:

$$P = \frac{1}{2} \int_{vol} \sigma E_{total}^2 dv \quad (1)$$

where σ is the conductivity (S/m) and $E_{total} = \|E_{total}\|$ is the amplitude of the total electric field (E_{total}) (V/m), which can be separated as two components:

$$E_{total} = -\frac{\partial A}{\partial t} - \nabla \phi = E_i + E_c \quad (2)$$

where A is the vector magnetic potential (Wb/m) and ϕ is the scalar electric potential (V), respectively. In order to reduce the total power absorbed by the sample, the E_{total} should be minimized, which means minimizing the components E_c and/or E_i .

2. Materials and Methods

2.1. Birdcage Head Coil

A high-pass (HP) birdcage head coil was modeled using

12 rods of 300 mm of length, disposed circularly with an inner diameter (ID) of 290 mm. To accurately simulate the field distribution generated by an ideal high-pass birdcage coil, 12 sinusoidal voltage sources of 1 V amplitude in series with a 50 Ω resistor were placed in both the top and bottom rings, in the middle of each of the segments between the rods of the coil (**Figure 1**). Each source was assigned a phase-shift equal to the azimuthal position of the segment (*i.e.*, 30°) between voltages in adjacent end ring segments, and with sources in opposite end rings having opposite orientation. The following frequencies were modeled: 12.8, 64, and 128 MHz, corresponding to 0.3, 1.5 and 3.0 T for water proton MRI.

2.2. Load: Phantom and Head Model

The birdcage head coil was loaded with a cylindrical sample having ID of 200 mm and length of 300 mm with a 5 mm resolution. Three different electrical properties for the phantom were simulated, namely: a) conductive sample ($\sigma = 0.2$ S/m, $\epsilon_r = 1$), b) dielectric sample ($\sigma = 0$ S/m, $\epsilon_r = 78$), and weak saline ($\sigma = 0.2$ S/m, $\epsilon_r = 78$) [6].

Simulations were also performed with an anatomically-precise human head model (**Figure 1**). The human head model was created by segmenting the digital photographic data of the National Library of Medicine's Visible Human Project [13, 14], and then transforming these segmented images into a 3D grid of Yee cell cubes [15]. The human head model had a $5 \times 5 \times 5$ mm³ isotropic resolution and contained 20 tissue types [16,17] having different conductivity (σ) and relative permittivity (ϵ_r) values.

2.3. Numerical Simulations and Data Processing

All simulations were performed using commercially available software (xFDTD, Remcom, Inc, State College, PA) and analysis of results was performed in Matlab (The MathWorks, Inc., Natick, MA). Simulation results of electromagnetic fields were normalized so that $\|B_1^+\| = 4 \mu\text{T}$ at the coil center corresponding to a 1.5 ms

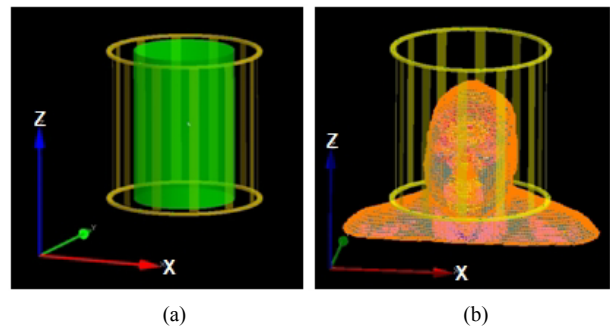


Figure 1. Geometry of high pass (HP) birdcage coil (yellow), sample (green, (a)) and head model (b) used for numerical simulations.

90° pulse [14].

The parameters used for the FDTD simulations to ensure convergence of the simulations were: 500,000 number of time steps, -30 dB convergence threshold, and 61.5 periods. The E_c and E_i separation method was applied only at the 12.8 MHz because the methods assumes quasi-static approximation. Calculation procedures for the method were developed and explained in [3] and are reported in the appendix for the reader's convenience.

3. Results

Figure 2 shows the normalized x-, y- and z-component of $|E_c|$, $|E_i|$, $|E_{total}|$ and $|B_i|$ within the empty coil in a single plane (YZ-plane) passing through the iso-center at 12.8 MHz. Values for $|E_i|$ were close to zero (*i.e.*, less than 0.04 V/m) along the axis of the RF coil, increasing with distance from the center line following Faraday's Law.

Table 1 reports the results of the simulations with the coil loaded with the conductive, dielectric, or weak saline phantom. There was approximately 25% reduction (*i.e.*,

56 vs. 76 V/m) in the average $|E_c|$ and 70% increase (*i.e.*, 231 vs. 134 V/m) in the maximum $|E_c|$ within the whole sample when the coil was loaded with the conductive, dielectric, or weak saline phantom compared to the empty coil.

Conversely, when comparing the results of the coil loaded with the head model vs. the empty coil, there was a 30% reduction (*i.e.*, 53 vs. 76 V/m) in the average $|E_c|$ and a 430% increase (*i.e.*, 716 vs. 134 V/m) for the maximum $|E_c|$, respectively (**Table 1**). Additionally, there was approximately a 20% reduction for average (*i.e.*, 63 vs. 53 V/m) and maximum $|E_i|$ (*i.e.*, 100 vs. 81 V/m) when comparing the empty coil vs. the coil loaded with the sample. Finally, when looking at the E_{total} , there was a destructive interference between E_c and E_i throughout the cylindrical sample or throughout the head, leading to an overall reduction of E_{total} (*i.e.*, 40 V/m in the empty coil vs. 20 V/m with the weak saline or 16 V/m in the Head).

Figure 3 and **Table 2** show the normalized y-component of the $|E_c|$, $|E_i|$, and $|E_{total}|$ at 12.8 MHz along the central sagittal plane (YZ-plane) with the coil empty,

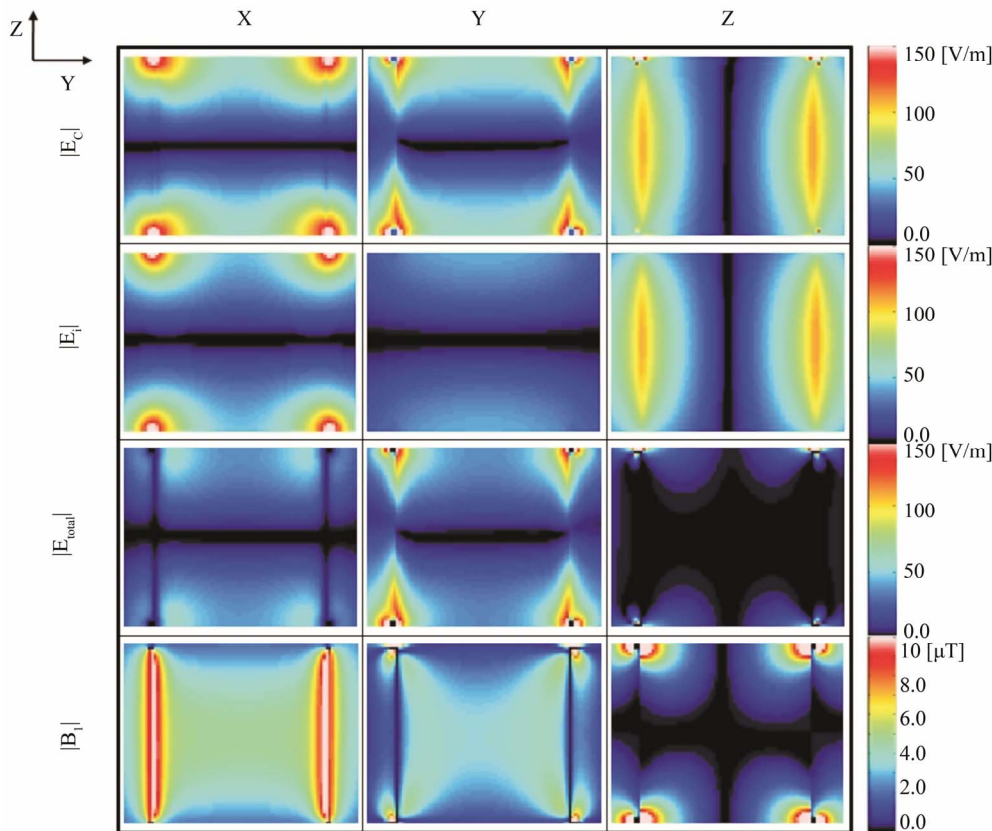


Figure 2. Magnitudes of x-, y-, and z-components of conservative E -field (E_c), magnetically-induced E -field (E_i), total E -field (E_{total}), and magnetic flux density (B_i) in the empty birdcage coil at 12.8 MHz. The coil was driven by a voltage source with a 50 Ω resistor and results were normalized to $|B_i^+| = 4 \mu\text{T}$ at the coil center.

Table 1. Normalized electromagnetic field properties within the whole sample when loaded with conductive (third row), dielectric (fourth row), weak saline (fifth row), and human head model (sixth row) using a high pass (HP) birdcage coil at 12.8 MHz. All values were normalized so that $|B_1^+| = 4 \mu\text{T}$ at the coil center.

12.8 MHz	$ B_1^+ $		$ E_c $		$ E_i $		$ E_{total} $	
	Mean [μT]	std [10^{-7}]	Mean [V/m]	Max [V/m]	Mean [V/m]	Max [V/m]	Mean [V/m]	Max [V/m]
Air	3.4	9.2	76	134	63	100	40	90
Conductive ($\sigma = 0.2, \epsilon_r = 1$)	3.5	7.5	56	231	52	81	20	210
Dielectric ($\sigma = 0, \epsilon_r = 78$)	3.5	7.5	56	221	51	81	21	199
Weak Saline ($\sigma = 0.2, \epsilon_r = 78$)	3.5	7.3	54	224	50	78	20	203
Head Model	2.5	15.2	53	716	49	109	16	693

Table 2. Normalized magnitude of 2D (YZ-plane) rotating RF magnetic field (B_1^+) and y-component of conservative E -field ($|E_{y,c}|$), magnetically induced E -field ($|E_{y,i}|$) and total E -field ($|E_y|$) between the coil and the sample in Figure 3. All values were normalized so that $|B_1^+| = 4 \mu\text{T}$ at the coil center.

12.8 MHz	$ B_1^+ $		$ E_{y,c} $		$ E_{y,i} $		$ E_y $	
	Mean [μT]	std [10^{-7}]	Mean [V/m]	Max [V/m]	Mean [V/m]	Max [V/m]	Mean [V/m]	Max [V/m]
Air	4.5	11.7	49	149	21	39	44	144
Conductive ($\sigma = 0.2, \epsilon_r = 1$)	4.3	9.4	76	165	17	32	73	163
Dielectric ($\sigma = 0, \epsilon_r = 78$)	4.2	9.4	73	161	17	32	71	159
Weak Saline ($\sigma = 0.2, \epsilon_r = 78$)	4.2	9.1	73	158	17	31	70	155

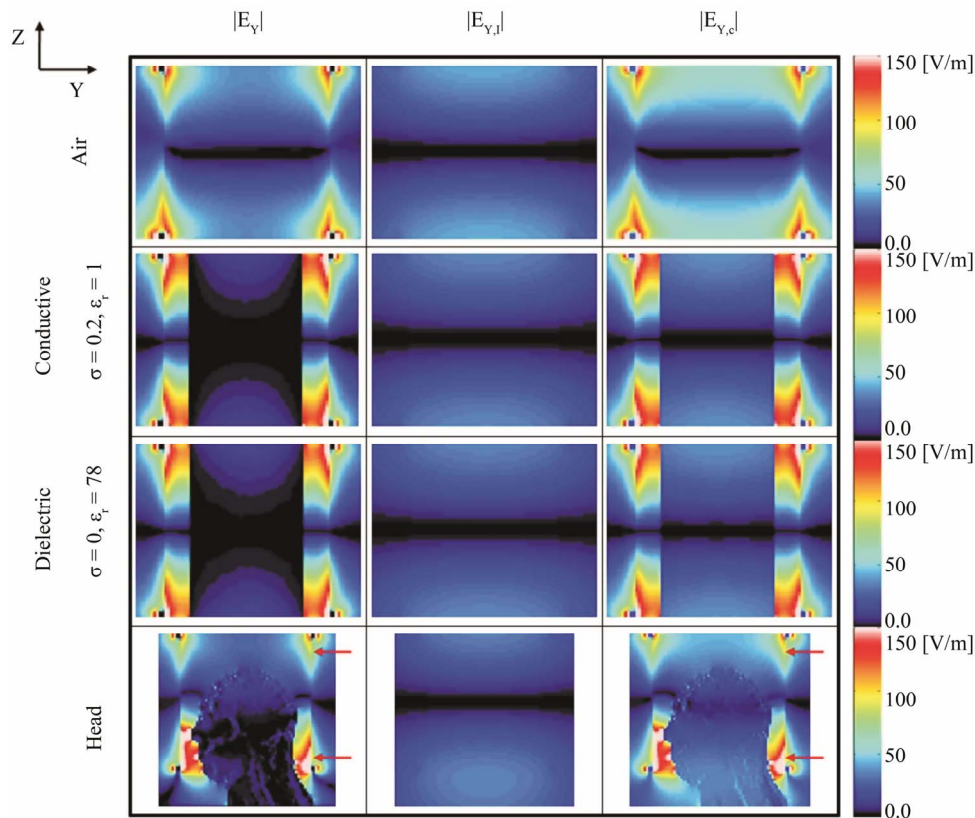


Figure 3. Calculated magnitude y-component of total E -field (E_y , first column), magnetically induced E -field ($E_{y,i}$, second column) and conservative E -field ($E_{y,c}$, third column) at 12.8 MHz when loaded with air (first row), conductive ($\sigma = 0.2 \text{ S/m}$, $\epsilon_r = 1$, second row), dielectric sample ($\sigma = 0 \text{ S/m}$, $\epsilon_r = 78$, third row) and human head model (fourth row). The z-directional size of a head image (fourth row) is longer than others to include neck and shoulder region. The weak saline images, similar to conductive or dielectric ones, are not shown in this figure.

loaded with the conductive, the dielectric phantom, and the head model. The change of electric field near the ending with and without the head model can be observed (red arrows in the fourth row). The electric field distribu-

tion for the conductive sample, the dielectric sample, and the weak saline (not shown) was very similar (see also **Table 3**).

Figure 4 and **Table 3** show the normalized z-compo-

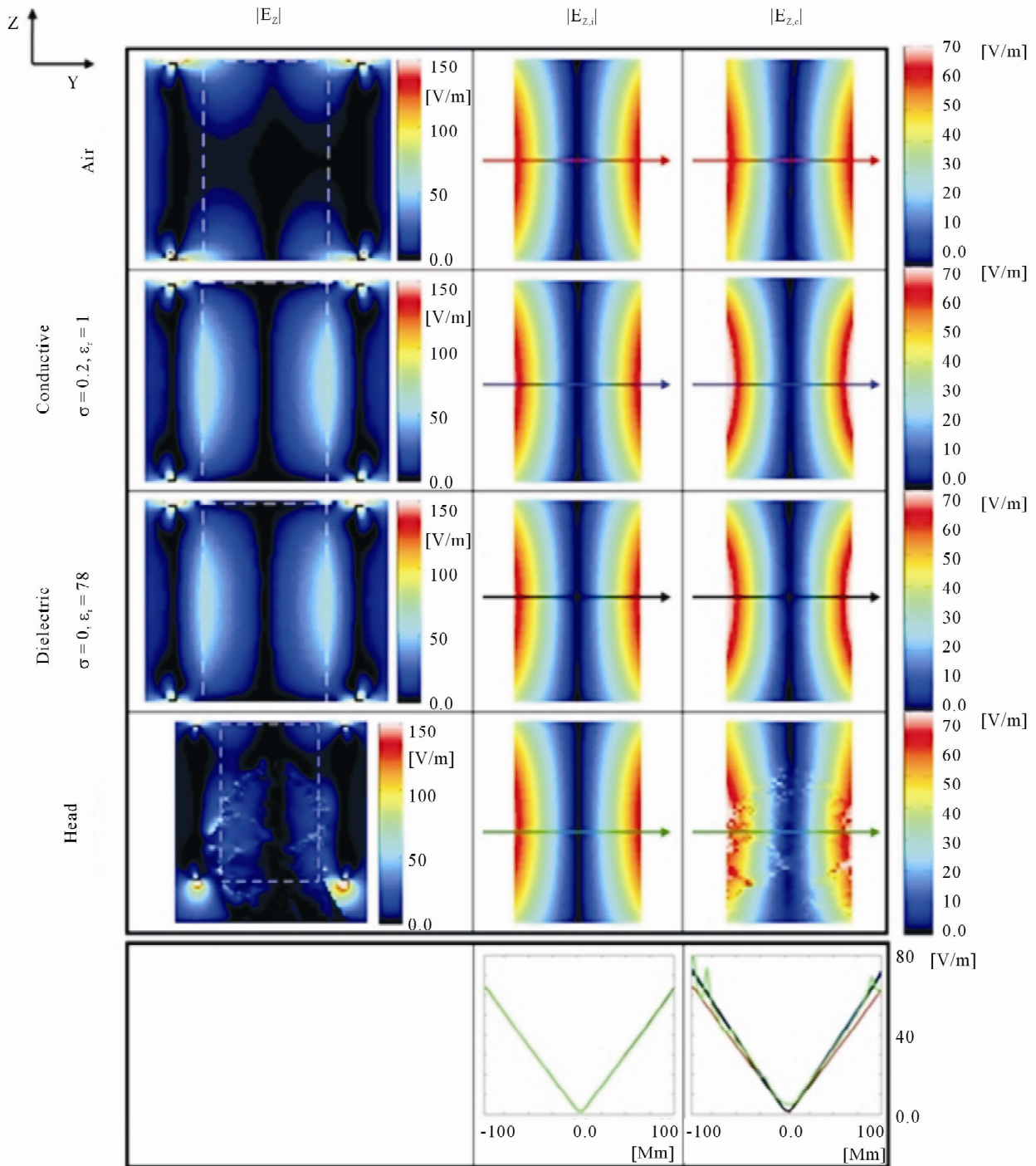


Figure 4. Calculated magnitude of E -field z-component at 12.8 MHz. Other parameters are same as Figure 3. Note that the magnitude of conservative E -field ($E_{z,c}$, third column) is increased when loaded with a conductive or a dielectric sample whereas no difference in magnetically-induced E -field ($E_{z,i}$, second column). White rectangular dotted lines in a first column indicate the region of a sample. The electric field distribution for the conductive sample, the dielectric sample, and the weak saline (not shown) was almost the same.

Table 3. Normalized magnitude of 2D (YZ-plane) rotating RF magnetic field (B_i^+) and z-component of conservative E -field ($E_{z,c}$), magnetically induced E -field ($E_{z,i}$) and total E -field (E_z) within the sample in Figure 4. Other parameters are same as Table 2.

12.8 MHz	$ B_i^+ $		$ E_{z,c} $		$ E_{z,i} $		$ E_z $	
	Mean [μ T]	std [10^{-7}]	Mean [V/m]	Max [V/m]	Mean [V/m]	Max [V/m]	Mean [V/m]	Max [V/m]
Air	3.3	9.0	29	67	29	67	4	31
Conductive ($\sigma = 0.2, \epsilon_r = 1$)	3.4	7.3	32	105	29	67	10	83
Dielectric ($\sigma = 0, \epsilon_r = 78$)	3.4	7.3	31	100	29	67	10	77
Weak Saline ($\sigma = 0.2, \epsilon_r = 78$)	3.4	7.1	31	105	29	67	10	83

ment of $|E_c|$, $|E_i|$, and $|E_{total}|$ at 12.8 MHz along the central sagittal plane (YZ-plane). The z-component of $|E_c|$ within the sample was increased of about 10% in average and 55% in maximum (Table 3) with addition of a conductive sample, a dielectric sample or a weak saline (not shown), whereas no changes were observed in the z-component of $|E_i|$.

Figure 5 shows the total magnitude of E_c , E_i , and E_{total} and rotating RF magnetic field (B_i^+ , fourth row) after normalization for the coil empty (first column), loaded with conductive cylinder (second column), dielectric cylinder (third column) and human head model (fourth column). For the coil loaded with conductive sample, dielectric sample, and weak saline (not shown), the $\|E_c\|$ and $\|E_{total}\|$ decreased within the sample, but increased in the space between sample and coil.

Figure 6 and Table 4 show the electromagnetic field as a function of frequency (12.8 MHz, 64 MHz, and 128 MHz) for the empty coil (first row), and the coil loaded with a weak-saline cylindrical sample (second row) and a head model (third row). As frequency increased from 12.8 MHz to 128 MHz, the average magnitude of total electric field within the weak saline sample (*i.e.*, mean $\|E\|_{sample}$) increased of about 390% (*i.e.*, 20 vs. 98 V/m). The fields for the coil loaded with a conductive or dielectric sample (not shown) were similar to the ones of the coil loaded with weak saline.

Figure 7 shows the calculated volume charge density ($\rho_v = \nabla \cdot \mathbf{D}$, where \mathbf{D} is the electric flux density) at the frequencies of 12.8 (first column), 64 (second column), and 128 MHz (third column) with different loading conditions. The charge density was highly concentrated on the surface of the sample or the head model regardless of the operating frequencies.

4. Discussion

For the empty coil, the z-component of the E_i —mainly caused by the currents flowing along the rungs—is dominant because E_i is perpendicular to the magnetic flux density (\mathbf{B}) following Faraday's Law (Figure 2). On

the sagittal plane (YZ-plane) the x-component of E_i mainly caused by the end-ring currents—was higher than the y-component; the comparison was reversed on the coronal planes.

The value of E_i at the center was zero (Figures 2-5), as expected given the specific electrical configuration of the coil and can be explained by means of the magnetic vector potential (A), proportional to the current density (J) (Equation (3)). Because opposite sides of a birdcage coil in ideal mode 1 resonance have equal J flowing in the opposite direction and generating an opposing A , the two A having same amplitude and opposite direction cancel each other out at the center. In these results, the value of electric field in the iso-center of the coil was very close to zero but not exactly zero (*i.e.*, 0.04 V/m, less than 0.2% of average total electric field within the whole sample). The E_c was significantly different when the coil was loaded with a conductive, a dielectric, a weak-saline sample, or a human head model, with approximately a 25% - 30% change in the average $\|E_c\|$ and up to 430% change in maximum $\|E_c\|$ within the whole sample (Table 1). This was due to the additional scalar potential (ϕ) within and surrounding the sample, as shown in Figure 3. When a conductive, dielectric, or weak-saline sample is located within the electric field generated by the RF coil, charged particles within the sample are moved to the boundaries of the sample, resulting in a polarization field which either has same or opposite direction of the original field depending on the specific region considered and on the components of the coil. Because of such polarization effects, the z-component of E_c ($|E_{z,c}|$) within the sample increased (Figure 4 and Table 3); however, because the additional scalar electric potential had opposite direction of the original one, the y-component of E_c ($|E_{y,c}|$) decreased within the sample. Moreover, because $|E_{y,c}|$ was the dominant component of the E_{total} , this resulted in an overall reduction in the E_{total} and an increase of magnetic field homogeneity within the sample (Figure 3, Tables 1 and 2). These results are in line with published literature [8,9,11]. However, the $|E_{y,c}|$ between a coil and

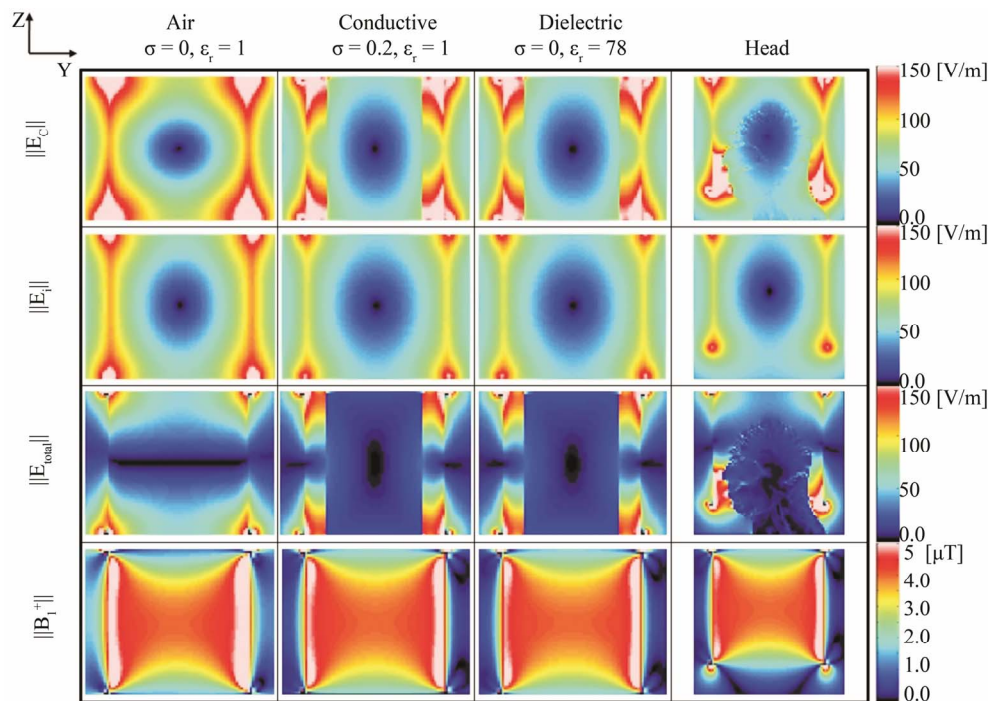


Figure 5. Total magnitude of conservative E -field (E_c , first row), magnetically-induced E -field (E_t , second row), total E -field (E_{total} , third row) and rotating RF magnetic field (B_1^+ , fourth row) after normalization when loaded with air (first column), conductive sample (second column), dielectric sample (third column) and human head model (fourth column). The z-directional size of a head image (fourth column) is longer than others to include neck and shoulder region. The electric field distribution for the conductive sample, the dielectric sample, and the weak saline (not shown) was almost the same.

Table 4. Results of the 3D electromagnetic simulations within the sample at the different frequencies evaluated in this study. Mean and standard deviation (std) of circularly polarized RF magnetic field ($|B_1^+|$) and total electric field ($|E|$) when loaded with air, weak saline and human head model at three different frequencies of 12.8, 64, and 128 MHz.

	$ B_1^+ _{\text{Sample}}$		Mean $ E _{\text{Sample}}$ [V/m]
	Mean [μT]	std [10^{-7}]	
Air (12.8 MHz)	3.4	9.2	40
Weak Saline (12.8 MHz)	3.5	7.3	20
Head (12.8 MHz)	2.5	15.2	16
Air (64 MHz)	3.6	6.9	159
Weak Saline (64 MHz)	2.9	7.1	85
Head (64 MHz)	2.3	14.4	75
Air (128 MHz)	3.6	6.4	315
Weak Saline (128 MHz)	1.5	8.4	98
Head (128 MHz)	1.9	12.7	119

a sample was increased because the additional scalar electric potential-due to the presence of the sample-had the same direction of the original one. This result extends previous published literature showing that the total electric field would decrease within the sample when the coil

is loaded with a conductive or a dielectric sample (as shown in (9,11)) (Table 1) and additionally demonstrating that the electric field increases between coil and the sample (Table 2). This result may have consequences on subject safety. For example, the accumulation of charge

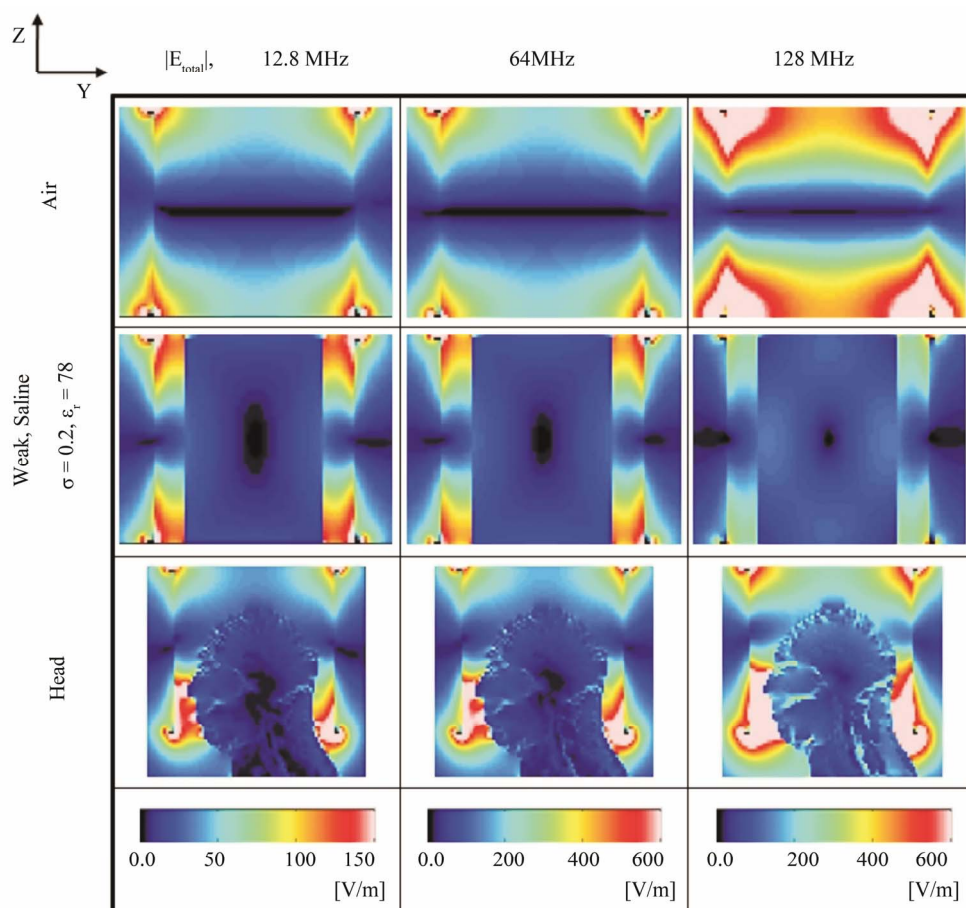


Figure 6. Calculated total magnitude of E -field ($|E_{total}|$) at three different frequencies of 12.8 (first column), 64 (second column), and 128 MHz (third column) for the empty coil (air—first row), and the coil loaded with a weak saline phantom (second row) and a human head model (third row). The z -directional size of a head image (third row) is longer than others to include neck and shoulder region.

on the boundary region of the sample may increase local and 10 g-average SAR. Moreover, when external conductive leads for physiological monitoring (e.g., ECG, EEG) are present, the increase in electric field between coil and sample may result in increasing induced currents along the monitoring leads, with possible increase of local SAR at the interface between leads and patient skin. Because of difficulties of SAR and temperature calculation in free space, direct comparisons of losses and heating in the objects were not studied.

The electric field variation of the x -component with addition of the samples was not shown in the figures because of the small absolute amplitude (less than 15% compared to the y - and z -component for the sagittal view) and because no difference was noticed among all the loading samples considered. Additionally, the results with a weak saline sample were similar to the results obtained with a conductive or a dielectric sample (Tables 2 and 3).

The change for the magnetically induced E -field (E_i)

with addition of the sample was much less when compared to E_c (i.e., about 13% - 18% change in the average $\|E_i\|$ and up to 22% change in the maximum $\|E_i\|$) (Table 1 and Figures 3-5). The reason that the value of E_i within and surrounding the sample appears to be relatively independent of sample properties at 12.8 MHz can be explained using Faraday's law. E_i is induced by a time varying vector magnetic potential (Equation (2)) which is mainly caused by the conduction current flowing in the RF coil. Because the RF coil used in this case is very small (300 mm in length and 290 mm ID) compared to the electrical wavelength (free space wavelength at 12.8 MHz equal to 23.4 m), the presence of the sample does not significantly affect the distribution of coil currents (no wavelength effect) and specifically E_i (Figure 5). However, as the frequency increased from 12.8 MHz to 128 MHz (free space wavelength equal to 2.34m), E_c and E_i both proportional to the frequency (Equation (2)) also increased and the E_{total} was much higher, (i.e., about 644% increase in average $\|E_{total}\|$

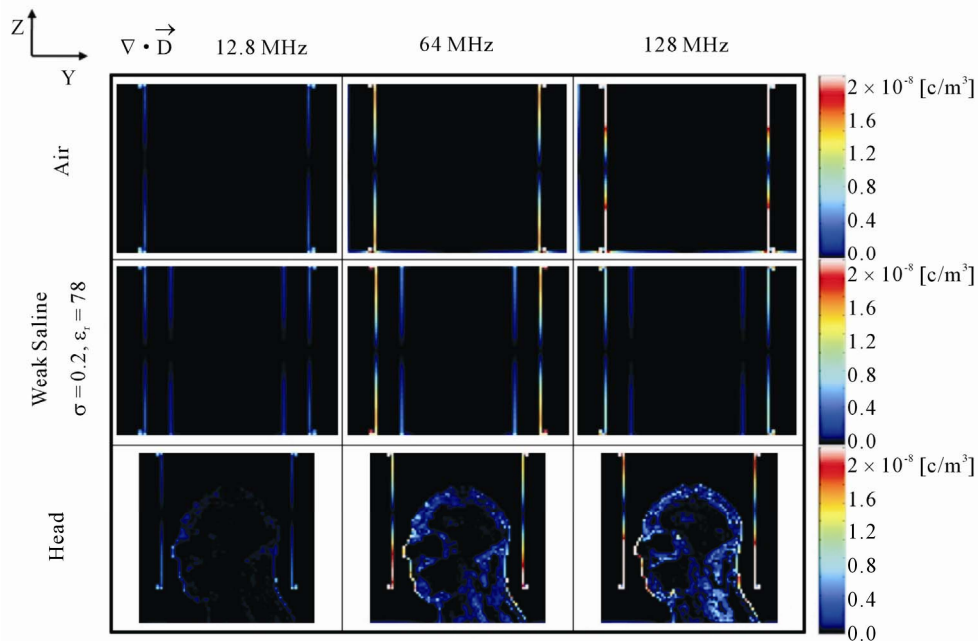


Figure 7. Calculated volume charge density ($\nabla \cdot D = \rho_v$) at the three frequencies of 12.8 (first column), 64 (second column), and 128 MHz (third column) with the empty coil (first row), and the coil loaded with weak-saline (second row) and head model (third row). The charge density distribution for the conductive sample (not shown), the dielectric sample (not shown), and the weak saline was almost the same.

within the head model compared to 12.8 MHz) (**Figure 6** and **Table 4**).

The calculated volume charge density in **Figure 7** was highly concentrated on the boundary region of the sample and the head model, matching well with the increased conservative electric field between the coil and the loading.

A previous study [6] showed that in a solenoid coil the E_c -shield can be used effectively to reduce E_{total} without changing B_1 because the direction of E_c -shield in the solenoid coil is orthogonal to the direction of current in the coil wires [6,8,9]. However, the results of this study show that the difference in current directions along the structure between a birdcage and a solenoid coil is significant enough to do not allow using the same E_c -shield approach with a birdcage coil.

5. Conclusion

This study presents the variations of electromagnetic field inside a birdcage coil when loaded with a conductive cylindrical sample, a dielectric cylindrical sample, a weak-saline cylindrical sample, or a head model. The results were presented using a designed E_c and E_i separation method at the frequency of 12.8 MHz. The additional scalar potential caused by the polarization effects within the load caused an increase of the y-component of E_c between coil and sample, and a decrease within the sample at 12.8 MHz resulting in higher possi-

bility of increased power deposition in the subject skin and induced RF currents in external leads used for physiological recording, *i.e.* ECG. The proposed E_c and E_i separation method can be applied as long as the current density in the RF coil is much greater than that in the sample and no significant wavelength effects are present for the accurate calculation of magnetic vector potential (A). As the frequency increased from 12.8 MHz to 128 MHz, the total E -field within and surrounding the sample increased significantly. Results indicate that the E_c -shield approach, previously proposed for a solenoid coil to reduce sample heating, cannot be used with a birdcage coil.

REFERENCES

- [1] International Electrotechnical Commission (IEC), "International Standard, Medical Equipment Part 2: Particular Requirements for the Safety of Magnetic Resonance Equipment for Medical Diagnosis," 3rd Edition, International Electrotechnical Commission, Geneva, Vol. 601, 2010, pp. 2-33.
- [2] "Guidance for Industry and FDA Staff: Criteria for Significant Risk Investigations of Magnetic Resonance Diagnostic Devices," 2003. <http://www.fda.gov/MedicalDevices/DeviceRegulationandGuidance/GuidanceDocuments/ucm072686.htm>
- [3] B. S. Park, A. G. Webb and C. M. Collins, "A Method to Separate Conservative and Magnetically-Induced Electric Fields in Calculations for MRI and MRS in Electrically-Small Samples," *Journal of Magnetic Resonance*,

- Vol. 199, No. 2, 2009, pp. 233-237.
[doi:10.1016/j.jmr.2009.05.007](https://doi.org/10.1016/j.jmr.2009.05.007)
- [4] D. I. Hoult and P. C. Lauterbur, "The Sensitivity of the Zeugmatographic Experiment Involving Human Samples," *Journal of Magnetic Resonance*, Vol. 34, No. 2, 1979, pp. 425-433.
- [5] W. Mao, B. A. Chronik, R. E. Feldman, M. B. Smith and C. M. Collins, "Consideration of Magnetically-Induced and Conservative Electric Fields within a Loaded Gradient Coil," *Magnetic Resonance in Medicine*, Vol. 55, No. 6, 2006, pp. 1424-1432. [doi:10.1002/mrm.20897](https://doi.org/10.1002/mrm.20897)
- [6] B. S. Park, T. Neuberger, A. G. Webb, D. C. Bigler and C. M. Collins, "Faraday Shields within a Solenoidal Coil to Reduce Sample Heating: Numerical Comparison of Designs and Experimental Verification," *Journal of Magnetic Resonance*, Vol. 202, No. 1, 2010, pp. 72-77. [doi:10.1016/j.jmr.2009.09.023](https://doi.org/10.1016/j.jmr.2009.09.023)
- [7] D. G. Gadian and F. N. H. Robinson, "Radiofrequency Losses on NMR Experiments on Electrically Conducting Samples," *Journal of Magnetic Resonance*, Vol. 34, No. 2, 1979, pp. 449-455.
- [8] A. Krahn, U. Priller, L. Emsley and F. Engelke, "Resonator with Reduced Sample Heating and Increased Homogeneity for Solid-State NMR," *Journal of Magnetic Resonance*, Vol. 191 No. 1, 2008, pp. 78-92. [doi:10.1016/j.jmr.2007.12.004](https://doi.org/10.1016/j.jmr.2007.12.004)
- [9] F. D. Doty, J. Kulkarni, C. Turner, G. Entzminger and A. Bielecki, "Using a Cross-Coil to Reduce RF Heating by an Order of Magnitude in Triple-Resonance Multinuclear MAS at High Fields," *Journal of Magnetic Resonance*, Vol. 128 No. 2, 2006, pp. 239-253. [doi:10.1016/j.jmr.2006.06.031](https://doi.org/10.1016/j.jmr.2006.06.031)
- [10] P. T. Hardy Jr. and K. M. Weil, "A Review of Thermal MR Injuries," *Radiologic Technology*, Vol. 81, No. 6, 2010, pp. 606-609.
- [11] Q. X. Yang, "A Method of Utilization of High Dielectric Constant (HDC) Materials for Reducing SAR and Enhancing SNR in MRI," US Patent No. 20,110,152,670, 2011.
- [12] K. R. Minard and R. A. Wind, "Solenoidal Microcoil design-Part II: Optimizing Winding Parameters for Maximum Signal-to-Noise Performance," *Nuclear Magnetic Resonance*, Vol. 13 No. 3, 2001, pp. 190-210. [doi:10.1002/cmr.1008](https://doi.org/10.1002/cmr.1008)
- [13] C. M. Collins and M. B. Smith, "Calculations of B_1 Distribution, SNR and SAR for a Surface Coil Adjacent to an Anatomically-Accurate Human Body Model," *Magnetic Resonance in Medicine*, Vol. 45, No. 4, 2001, pp. 692-699. [doi:10.1002/mrm.1092](https://doi.org/10.1002/mrm.1092)
- [14] C. M. Collins and M. B. Smith, "Signal-to-Noise Ratio and Absorbed Power as Functions of Main Magnetic Field Strength, and Definition of '90°' RF Pulse for the Head in the Birdcage Coil," *Magnetic Resonance in Medicine*, Vol. 45, No. 4, 2001, pp. 684-691. [doi:10.1002/mrm.1091](https://doi.org/10.1002/mrm.1091)
- [15] K. Yee, "Numerical Solution of Initial Boundary Value Problems Involving Maxwell's Equations in Isotropic media," *IEEE Transactions on Antennas and Propagation*, Vol. 14, No. 3, 1966, pp. 302-307. [doi:10.1109/TAP.1966.1138693](https://doi.org/10.1109/TAP.1966.1138693)
- [16] C. Gabriel, T. Y. A. Chan and E. H. Grant, "Admittance Models for Open Ended Coaxial Probes and Their Place in Dielectric Spectroscopy," *Physics in Medicine and Biology*, Vol. 39, No. 12, 1994, pp. 2183-2200. [doi:10.1088/0031-9155/39/12/004](https://doi.org/10.1088/0031-9155/39/12/004)
- [17] Federal Communication Commission (FCC), "Body Tissue Dielectric Parameters," 2010. <http://transition.fcc.gov/oet/rfsafety/dielectric.html>